DALTON
FULL PAPER

Synthesis, spectroscopic and electrochemical properties of mononuclear and dinuclear bis(bipy)ruthenium(II) complexes containing dimethoxyphenyl(pyridin-2-yl)-1,2,4-triazole ligands †

Paolo Passaniti,[a] Wesley R. Browne,[b] Fiona C. Lynch,[b] Donal Hughes,[b] Mark Nieuwenhuyzen,[c] Paraic James,[d] Mauro Maestri[a] and Johannes G. Vos*[b]

[a] *Dipartimento di Chimica "G.Ciamician", University of Bologna Via Selmi 2, 40126 Bologna, Italy*
[b] *National Centre for Sensor Research, School of Chemical Sciences, Dublin City University, Dublin 9, Ireland. E-mail: johannes.vos@dcu.ie*
[c] *School of Chemistry, Queen's University of Belfast, Belfast, Northern Ireland, UK BT9 5AG*
[d] *National Institute for Cellular Biotechnology, Dublin City University, Dublin 9, Ireland*

Received 25th September 2001, Accepted 12th February 2002
First published as an Advance Article on the web 26th March 2002

The ligands **HL1** and $\mathbf{H_2L2}$ and the complexes $[Ru(bipy)_2L1]PF_6\cdot 2H_2O$ **1**, $[(Ru(bipy)_2)_2L2](PF_6)_2\cdot 7H_2O$ **2**, {where **HL1** = 3-(2′,5′-dimethoxyphenyl)-5-(pyridin-2″-yl)-1H-1,2,4-triazole, $\mathbf{H_2L2}$ = 1,4-bis(5′-(pyridin-2″-yl)-1′H-1′,2′,4′-triazol-3′-yl)-2,5-dimethoxybenzene and bipy = 2,2′-bipyridyl}, have been prepared and characterised, by NMR, UV–vis and emission spectroscopies and by electrochemical measurements. X-Ray crystal structures of ligands **HL1**, $\mathbf{H_2L2}$ and of the complex **1** are also reported. The dinuclear complex (**2**) exhibits a weak electronic interaction between the metal centres, which is modulated by the protonation state of the 1,2,4-triazole rings. The extent of the metal–metal interaction in these systems is compared with that observed in other pyridyl-1,2,4-triazole based dinuclear compounds of differing metal–metal distances.

Introduction

Ruthenium(II) polypyridyl complexes are of interest for their spectroscopic, photophysical, photochemical, and electrochemical properties.[1–3] These properties are of particular use in the construction of supramolecular systems and photochemically driven molecular devices.[4,5] Ruthenium(II) polypyridyl complexes have also received extensive attention as models for photo-system II and in the catalytic photochemical cleavage of water.[6]

Of particular interest is the design of multinuclear structures capable of directing and modulating electron and energy transfer processes.[4,5] In this regard many studies of ruthenium complexes covalently bound to electron acceptors or donors have been reported. The general approach taken in electron transfer studies has been to bind the electron acceptor/donor to the ruthenium polypyridyl centre *via* the polypyridyl ligands.[7–9] However, since the excited state in such compounds is normally based on these ligands a strong coupling between the metal centre and the electron donor/acceptor is usually observed, which precludes a long-lived charge separation.[9,10] In our laboratories we have taken a different approach aimed at weakening the direct electronic coupling between the electron donor/acceptor and the sensitiser, consequently slowing down the back reaction and achieving a longer lived charge separated state.[11] This approach is based on the attachment of groupings to spectator ligands, such as 3-(pyridin-2′-yl)-1,2,4-triazoles. In addition, the pH dependent properties of the 1,2,4-triazole ligands are shown to be useful in applications such as molecular switches.[12]

Due to its role as redox relay in biological systems, the hydroquinone/quinone redox couple is of particular interest. In an earlier study on ruthenium polypyridyl complexes incorporating pyridyltriazole ligands with pendent hydroquinone groupings an electrochemically induced intramolecular protonation of the ruthenium centre was observed upon oxidation of the hydroquinone.[13] We are presently involved in a systematic study of this unusual observation and also of the photophysical properties of molecular dyads of this type. In the present contribution, the spectroscopic and electrochemical properties of the mono-nuclear complex **1** based on the $Ru(bipy)_2$-complex of 3-(2′,5′-dimethoxyphenyl)-5-(pyridin-2″-yl)-1H-1,2,4-triazole (**HL1**) and the dinuclear complex **2** based on the $Ru(bipy)_2$-complex of 1,4-bis(5′-(pyridin-2″-yl)-1′H-1′,2′,4′-triazol-3′-yl)-(2,5-dimethoxybenzene) ($\mathbf{H_2L2}$) are reported (bipy = 2,2′-bipyridyl). The electrochemical, spectroelectrochemical and photophysical properties of the compounds are compared with those reported for analogous mononuclear and dinuclear complexes based on 3-(pyridin-2′-yl)-1H-1,2,4-triazole (Hpytr) (**3**) and 3,5-bis(pyridin-2′-yl)-1H-1,2,4-triazole (Hbpt) (**4**). For structures of complexes **1**–**4** see Fig. 1. The compounds reported are synthetic precursors to the analogous hydroquinone/quinone compounds and serve as model compounds. The results obtained for the hydroquinone/quinone analogues will be reported in a further publication.

Experimental

Materials

All solvents employed were of HPLC grade or better and used as received unless otherwise stated. For all spectroscopic measurements Uvasol (Merck) grade solvents were employed. All reagents employed in synthetic procedures were of reagent grade or better. *Cis*-$[Ru(bipy)_2Cl_2]\cdot 2H_2O$,[14] (pyridin-2-yl)-

† Electronic supplementary information (ESI) available: figures showing the molecular structures and intermolecular interactions for **HL1** and $\mathbf{H_2L2}$; ^{1}H COSY NMR spectrum of **2**. See http://www.rsc.org/suppdata/dt/b1/b108728m/

 DOI: 10.1039/b108728m

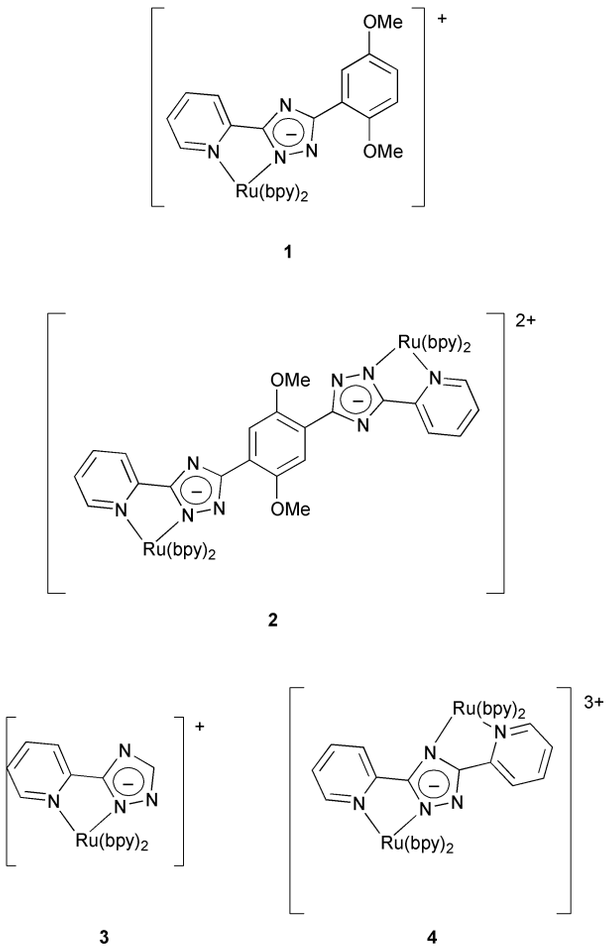

Fig. 1 Structures of compounds **1**–**4**.

amidrazone and tetraethylammoniumperchlorate (TEAP)[15] were prepared by previously reported procedures.

Syntheses

3-(2′,5′-Dimethoxyphenyl)-5-(pyridin-2″-yl)-1H-1,2,4-triazole (HL1). 2,5-Dimethoxybenzoic acid (10 g, 55 mmol) and PCl_5 (11.45 g, 55 mmol) were reacted together to form a clear yellow product. The $POCl_3$ formed was removed by distillation with slight heating (40 °C) under a weak vacuum leaving a clear yellow liquid, which crystallised overnight under vacuum. The acid chloride (11.03 g, 50 mmol) formed was dissolved in 30 cm^3 of dry tetrahydrofuran and added dropwise to (pyridin-2-yl)amidrazone (6.85 g, 50 mmol) and sodium carbonate (2.65 g, 25 mmol) in 40 cm^3 of tetrahydrofuran, resulting in immediate precipitation of the pale yellow acylamidrazone. The reaction mixture was stirred for a further 4 h and the yellow product collected by vacuum filtration and stirred in ice water for 30 min followed by recovery using vacuum filtration. The yellow product was dried overnight at 80 °C. Yield of 1-(2′,5′-dimethoxyphenyl)-4-(pyridin-2″-yl)acylamidrazone: 10.95 g, (73%), mp 190 °C. The amidrazone (6 g, 20 mmol) was dissolved in a minimum of ethylene glycol and heated at reflux for 30 min. On cooling, the ligand **HL1** precipitated from solution and was collected by filtration. The product was decolourised over charcoal and crystallised from dichloromethane. Yield: 3.4 g, 60%. ^{1}H NMR (d_6-acetone): δ 12.54 (1H, s), 8.69 (1H, d, 3.9 Hz), 8.20 (1H, d, 7.9 Hz), 7.87 (1H, t, 7.9 Hz), 7.82 (1H, s, 3.0 Hz), 7.39 (1H, t, 4.9 Hz), 7.12 (1H, d, 9.9 Hz), 7.04 (1H, dd, 3.0 Hz, 8.9 Hz), 3.99 (3H, broad s), 3.83 (3H, s). Elemental analysis: Found (Calc. for $C_{15}H_{14}N_4O_2$) C 63.62 (63.83), H 5.15 (4.96), N 18.74 (19.86)%.

1,4-Bis(5′-(pyridin-2″-yl)-1′H-1′,2′,4′-triazol-3′-yl)-2,5-dimethoxybenzene (H_2L2). Diethyl-2,5-dihydroxyterephthalate (5.09 g, 20 mmol) and potassium carbonate (13.8 g, 100 mmol) were stirred with 100 cm^3 dry acetone in a flask fitted with reflux condenser and $CaCl_2$ drying tube. Iodomethane (14.2 g, 100 mmol) was added and the mixture heated to reflux for 48 h. The reaction was followed by TLC (mobile phase: pet. ether (40/60) : diethyl ether 2 : 1 v/v). On cooling, the white precipitate was filtered and washed with acetone. Yield of diethyl-2,5-dimethoxyterephthalate: 5.36 g (95%). ^{1}H NMR (d_1-chloroform): δ 7.36 (1H, s), 4.36 (2H, q, 7.4 Hz), 3.87 (3H, s), 1.37 (3H, t, 7.4 Hz).

Diethyl-2,5-dimethoxyterephthalate (5 g, 18 mmol) was added to 5 g (9 mmol) of potassium hydroxide in 15 cm^3 ethylene glycol, and heated at 100 °C until the mixture became homogenous. The ethanol formed during heating was removed by distillation at reduced pressure. The reaction mixture was then cooled, H_2O (20 cm^3) was then added and the reaction mixture was made slightly acidic by the addition of 20% H_2SO_4, which resulted in a white precipitate of 2,5-dimethoxyterephthalatic acid forming. This was filtered and washed with water (10 cm^3) and then acetone (5 cm^3). The 2,5-dimethoxyterephthalatic acid was dried in a Kugelrohr apparatus *in vacuo* over P_2O_5 at 100 °C. Yield: 3.9 g (94%), mp 265 °C. ^{1}H NMR (d_6-dimethylsulfoxide): δ 7.28 (1H, s), 3.77 (3H, s).

Phosphorous pentachloride (6.25 g, 30 mmol) was added to 2,5-dimethoxyterephthalic acid (3.5 g, 15 mmol) and the solids stirred with gentle heating. After evolution of gas had ceased, the phosphoryl oxychloride was removed by distillation at normal pressure and then under reduced pressure. The 2,5-dimethoxyterephthaloyl dichloride (3.95 g, 15 mmol) formed was dissolved in 50 cm^3 tetrahydrofuran and added with stirring to a solution of (pyridin-2-yl)amidrazone (4.76 g, 35 mmol) and sodium carbonate (1.59 g, 15 mmol) in 30 cm^3 of dry tetrahydrofuran at 0 °C. After stirring for 24 h, the reaction contents were added to 100 g of ice water and stirred for 30 min. The yellow solid was filtered, washed with water and acetone, and dried under vacuum. Impurities were removed by heating the crude product in dimethylsulfoxide, filtering and washing with acetone (10 cm^3). Yield of 1,4-bis(acylpyridin-2′-ylamidrazone)-2,5-dimethoxybenzene: 5 g (10 mmol, 67%), mp 189 °C. ^{1}H NMR (d_6-dimethylsulfoxide): δ 10.21 (2H, s, –NH), 8.61 (2H, d, 5.6 Hz, H6), 8.17 (2H, d, 7.4 Hz, H3), 7.76 (2H, t, 7.4 Hz, H4), 7.50(2H, t, 7.4 Hz, H5), 7.38 (2H, s, Benz-H), 6.81(4H, s, $-NH_2$), 4.03 (6H, s, $-OCH_3$).

1,4-Bis(acylpyridin-2′-ylamidrazone)-2,5-dimethoxybenzene (5 g, 10 mmol) was heated to reflux in ethylene glycol until the reaction mixture turned to a clear brown colour. The product (**H_2L2**), a tan solid, precipitated from solution overnight and was recrystallised from dimethylsulfoxide. Yield of **H_2L2**: 2.3 g (5.4 mmol, 54%). ^{1}H NMR (d_6-dimethylsulfoxide): δ 14.11 (2H, broad s, –NH), 8.70 (2H, broad s, H6), 8.18 (2H, d, H3), 7.94 (4H, broad s, H4 and Benz-H); 7.47 (2H, s, H5); 4.03 (6H, broad s, $-OCH_3$). Elemental analysis: Found (Calc. for $C_{22}H_{18}N_8O_2 \cdot 1H_2O$) C 59.46 (59.46), H 4.20 (4.50), N 25.42 (25.23)%.

[Ru(bipy)$_2$(L1)]PF$_6$·2H$_2$O (1). *Cis*-[Ru(bipy)$_2$Cl$_2$]·2H$_2$O (370 mg, 0.71 mmol) and **HL1** (200 mg, 0.71 mmol) were heated at reflux for 8 h in 150 cm^3 EtOH–H_2O (2 : 1 v/v). The hot solution was filtered and evaporated to dryness after which 10 cm^3 of water was added to the dark red product. **1** was precipitated with an excess aqueous solution of NH_4PF_6. The product was purified by column chromatography with activated neutral alumina (Brockmann 1, std grade, 150 mesh, Aldrich) and acetonitrile as eluent. The product obtained was recrystallised from acetone–H_2O (with 1 drop of conc. ammonia). Single crystals for X-ray structure determination were grown from an acetone solution of the product. Yield: 495 mg (82%). ^{1}H NMR (d_3-acetonitrile). δ 8.45 (2H, t, 8.9 Hz), 8.38 (2H, t, 8.9 Hz), 8.08

Table 1 X-Ray experimental crystal data for **HL1**, H_2L2 and **1**

	HL1	**H_2L2**	**1**
Empirical formula	$C_{15}H_{14}N_4O_2$	$C_{22}H_{18}N_8O_2$	$C_{38}H_{35}F_6N_8O_3PRu$
M/g mol^{-1}	282.30	426.44	897.78
T/K	293(2)	153(2)	293(2)
Wavelength/Å	1.54178	0.71073	1.54178
Crystal system, space group	Monoclinic, $P2_1/n$	Monoclinic, $P2_1/c$	Triclinic, $P\bar{1}$
a/Å, α/°	10.664(2), 90	9.235(3), 90	11.704(7), 69.92
b/Å, β/°	17.689(7), 96.96	11.636(3), 106.44	12.915(7), 88.60
c/Å, γ/°	15.057(3), 90	10.096(3), 90	15.631(9), 63.14
V/Å^3, Z	2819.4(14), 8	1040.5(5), 2	1956(2), 2
Crystal dimensions/mm	0.85 × 0.19 × 0.12	0.76 × 0.21 × 0.30	0.32 × 0.11 × 0.15
μ/mm^{-1}	0.754	0.093	4.358
No. reflections collected	3763	1853	7006
Independent reflec. (R_{int})	3540 (0.0549)	1359 (0.0528)	4917 (0.0501)
Final R indices [$I > 2\sigma(I)$] $R1$ ($wR2$)	0.065 (0.1599)	0.0610 (0.0991)	0.0655 (0.1639)
R indices all data $R1$ ($wR2$)	0.1103 (0.1952)	0.1398 (0.1258)	0.0761 (0.1724)

(1H, d, 7.9Hz, H3), 7.95 (7H, m, containing H4), 7.79 (2H, t, 4.9 Hz), 7.51 (1H, d, 5.9 Hz, H6), 7.42(1H, t, 6.9 Hz), 7.38 (2H, t, 5.9 Hz), 7.27 (1H, t, 5.9 Hz), 7.20 (1H, d, 2.9 Hz, H3″), 7.12 (1H, t, 6.9 Hz, H5), 6.93 (1H, d, 8.9 Hz, H6″), 6.83 (1H, dd, 2.9 Hz, 8.9, H5″), 3.71(3H, s, –OCH_3 1″), 3.61(3H, s, –OCH_3 4″). Elemental analysis: Found (Calc. for $C_{35}H_{33}N_8O_4PF_6Ru$) C 48.2 (48.0), H 4.0 (3.8), N 12.4 (12.8)%.

[(Ru(bipy)$_2$)$_2$(L2)](PF$_6$)$_2$·7H$_2$O (2). 2 was prepared in a similar manner to **1**, except that 0.25 g (0.48 mmol) of *cis*-[Ru(bipy)$_2$(Cl)$_2$]·2H$_2$O was heated at reflux with 0.1 g (0.24 mmol) of **H_2L2**. Yield: 0.32 g (89%). ^{1}H NMR (d_3-acetonitrile): δ 8.47 (2H, d, 7.4 Hz), 8.68 (2H, d, 7.4Hz), 8.59 (4H, t, 7.4 Hz), 8.29 (2H, d, 7.4 Hz, H3), 8.07 (8H, m), 7.96 (10H, m, H4), 7.71 (2H, d, 5.5 Hz, H6), 7.50 (8H, m, Benz-H), 7.37 (2H, t, 7.4 Hz), 7.24 (2H, t, 7.4 Hz, H5), 3.54 (6H,s,–OCH_3). Elemental analysis: Found (Calc. for $C_{62}H_{62}N_{18}O_9P_2F_{12}Ru_2$) C 44.7 (44.65), H 3.4 (3.72), N 13.1 (13.44)%.

Elemental analysis was performed at the Microanalytical Laboratory at University College Dublin.

X-Ray crystallography

Data for **HL1**, **H_2L2** and **1** were collected on a Siemens P4 diffractometer using the XSCANS[16] software with graphite monochromated Mo-K_α radiation (Table 1) Relevant experimental data is presented in Table 1.

The structures were solved using direct methods and refined with the SHELXTLPC and SHELXL-93 program packages[17] and the non-hydrogen atoms were refined with anisotropic thermal parameters.

CCDC reference numbers 171755–171757.

See http://www.rsc.org/suppdata/dt/b1/b108728m/ for crystallographic data in CIF or other electronic format.

NMR spectroscopy

^{1}H and ^{1}H COSY spectra were recorded on a Bruker AC400 (400 MHz) NMR spectrometer. All measurements were carried out in d_6-dimethylsulfoxide, d_1-chloroform or d_6-acetone for ligands and d_3-acetonitrile for complexes. Peak positions are relative to residual solvent peaks.

Photophysical measurements

UV-vis absorption spectra were recorded on a Shimadzu UV.vis-NIR 3100 spectrophotometer interfaced with an Elonex-466 PC using UV-vis data manager software. Emission spectra were recorded using a LS50-B Luminescence spectrophotometer, equipped with a red sensitive Hamamatsu R928 PMT detector, interfaced with an Elonex-466 PC using Windows based fluorescence data manager software. Emission/excitation slit widths were 5 nm. Emission spectra are uncorrected for photomultiplier response. 1 cm path length quartz cells were used for recording spectra. Luminescence lifetime measurements were obtained using an Edinburgh Analytical Instruments (EAI) Time Correlated Single Photon Counting apparatus (TCSPC) comprising of two model J-yA monochromators (emission and excitation), a single photon photomultiplier detection system model 5300, and a F900 nanosecond flashlamp (N_2 filled at 1.1 atm pressure), interfaced with a personal computer *via* a Norland MCA card. Data correlation and manipulation was carried out using EAI F900 software version 5.1.3. Emission lifetimes were calculated using a single exponential fitting function (Edinburgh instruments F900 software). pH titrations of **1** and **2** were carried out in Britton–Robinson buffer (0.04 M H_3BO_3, 0.04 M H_3PO_4, 0.04 M CH_3CO_2H) (pH was adjusted using concentrated sulfuric acid or sodium hydroxide solution). The appropriate isosbestic point from the absorption spectra was used as the excitation wavelength for emission titrations.

Electrochemical and spectroelectrochemical measurements

Electrochemical measurements were carried out on a Model 660 Electrochemical Workstation (CH Instruments). Typical complex concentrations were 0.5 to 1 mM in anhydrous acetonitrile (Aldrich 99.8%) containing 0.1 M TEAP. A Teflon shrouded glassy carbon working electrode, a Pt wire auxiliary electrode and SCE reference electrode were employed. Solutions for reduction measurements were deoxygenated by purging with N_2 or Ar gas for 15 min prior to the measurement. Measurements were made in the range of −2.0 to 2.0 V (w.r.t SCE electrode). Protonation of complexes was achieved by addition of 0.1 M trifluoroacetic acid (in acetonitrile) to the electrolyte solution. The scan rates used were typically 100 or 200 mV s^{-1}. Spectroelectrochemistry was carried out using an OTTLE set-up comprising of a home made Pyrex glass, thin layer cell (1 mm pathlength). The optically transparent working electrode was made from platinum–rhodium gauze, the counter electrode used was a platinum wire, and the reference electrode was a pseudo Ag/AgCl reference electrode. 0.1 M TEAP in anhydrous acetonitrile was used as electrolyte. The working electrode was held at the required potential throughout the measurement using an EG&G PAR Model 363 potentiostat. Absorption and emission spectra were recorded as described above.

Results and discussion

As noted in the introduction, the ultimate aim of our investigations is the study of metal complexes having pendent hydroquinone or quinone groupings. In earlier studies hydroquinone type ligands such as the hydroquinone analogue of **HL1**, 3-(2′,5′-dihydroxyphenyl)-5-(pyridin-2″-yl)-1,2,4-triazole were

prepared directly using 2,5-dihydroxybenzoic acid.[13] With this approach however, low yields were generally obtained. For this reason a new synthesis has been developed based on methoxy precursors with subsequent deprotection of these groups to form the required hydroquinone complex. In this contribution we report on the synthesis and properties of these dimethoxy-'protected' complexes. The synthesis of the ligands **HL1** and **H_2L2** and complexes **1** and **2** (Fig. 1) have been carried out by modification of general procedures.[18] In this manner dimethoxy precursors can be obtained in high yield.

X-Ray crystallography

The molecular structures obtained for **HL1** and **H_2L2** confirm the structural features of the two ligands. Figures showing the molecular structure and intermolecular interactions are given as ESI.† The molecular structure of **1** is shown in Fig. 2. In the

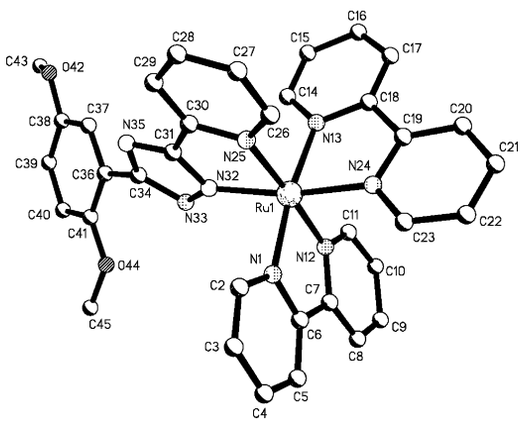

Fig. 2 Molecular structure and labelling scheme for **1**.

X-ray analysis of **1** the protons on one of the methoxy groups are disordered. Complex **1** cocrystallised with a molecule of acetone and a hexafluorophosphate counter anion. From the crystal structure it is clear that the ligand is bound through the pyridine-N and N2 of the triazole ring (or *via* N(25) and N(32)). The bite angle of the N(25)–Ru(1)–N(32) is 77.8(2)°, which corresponds well with the bite angle of 77.9(1)° obtained by Hage *et al.* for [Ru(bipy)$_2$(3-(2-hydroxy-phenyl)-5-(pyridin-2-yl)-1,2,4-triazole)]PF_6·CH_3COCH_3.[19] Bite angles of 79.5(3) and 78.8(3)° for bipyridine ligands and Ru–N distances of 2.033(7)–2.098(7) Å are also comparable to those found in other complexes.[19,20] Ru(1)–N(25) at 2.098(7) Å is the longest Ru–N bond in the complex. One factor contributing to this increased length is limited π-backbonding to the π-electron rich 1,2,4-triazole ring from the metal centre. The intermolecular X-ray structure is dominated by interaction between two C(3)–H atoms and the N2 nitrogen of the triazole ring forming a hydrogen bonded dimer (Fig. 3). The dimers form a three-dimensional network *via* π ··· π interactions and hydrogen bonding involving the bipy and pyridyltriazole ligands. The packing of these dimers creates cavities within the lattice in which the PF_6 anions and acetone molecules are located.

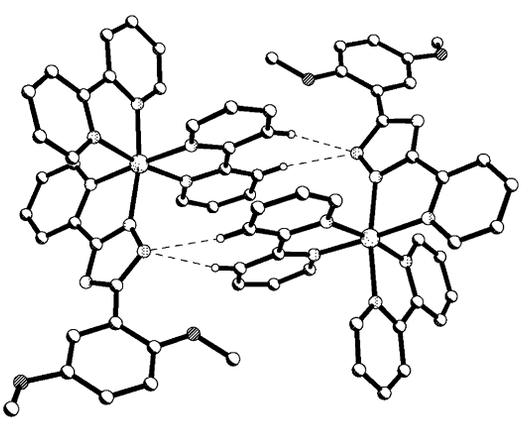

Fig. 3 Diagram of the hydrogen bonded dimer for **1**.

^{1}H NMR spectroscopy

^{1}H NMR spectra have been used extensively to determine the coordination mode of pyridyltriazoles and other types of chelating ligands.[21] The spectra obtained for **1** and **2** are shown in Fig. 4. Due to the complexity of the ^{1}H NMR spectra of the

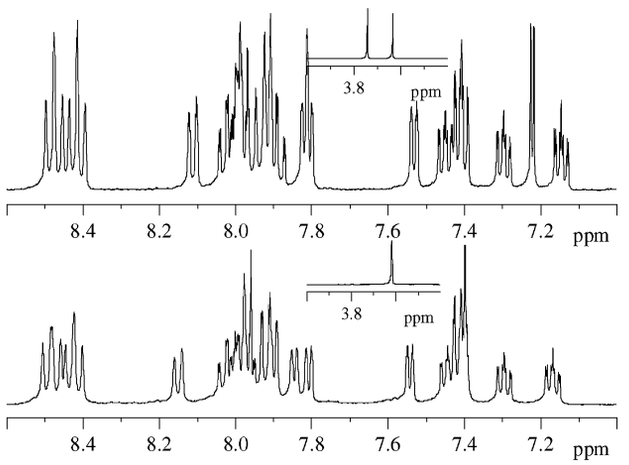

Fig. 4 ^{1}H NMR spectra of **1** (upper spectrum) and **2** (lower spectrum) in d_3-acetonitrile (400 MHz). –OCH_3 signals are shown as insets.

complexes ^{1}H COSY NMR spectroscopy (see ESI†) has been performed of both ligands and complexes and the spectra have been assigned by comparison with data previously reported for similar ligands and complexes.[21] It is worth pointing out that for **1** two non-equivalent methoxy signals are observed at 3.61 and 3.74 ppm. The spectrum obtained for **2** is strikingly simple. The dinuclear compound obtained is clearly highly symmetric as indicated by the presence of only one methoxy signal at 3.64 ppm and by the fact that the phenyl protons are equivalent and found as a singlet at 7.40 ppm. In contrast for the mononuclear complex **1** the three phenyl protons are all non-equivalent and appear at 6.83, 6.93 and 7.20 ppm. The crystal structure obtained for **1** (Fig. 2) shows that the coordination mode of the triazole ring in this compound is *via* the N2 nitrogen atom. For **3** it has been shown previously that the ^{1}H NMR spectra of the N2 and N4 bound coordination isomers are significantly different.[21] The symmetric ^{1}H NMR of **2** together with steric considerations and its similarity with the spectrum of **1**, point therefore strongly to a N2 coordination of both the 1,2,4-triazole rings in the dinuclear species.

Photophysical and acid–base properties

The photophysical data obtained for **1** and **2** are summarised in Table 2, together with data for $[Ru(bipy)_3]^{2+}$ and complexes **3** and **4** for comparison. For both **1** and **2**, the absorption and emission maxima are red-shifted with respect to $[Ru(bipy)_3]^{2+}$ [1] but are in agreement with those reported for **3** and **4**.[21] This is not unexpected as π-electron rich 1,2,4-triazole containing ligands such as **HL1** and **H_2L** are stronger σ-donors and weaker π-acceptors than 2,2′-bipyridine and destabilise the filled metal d-orbitals and hence raise the energy of the ground state metal based orbitals.[21] On protonation of both **1** and **2** a blue shift of both the lowest energy absorption bands and the emission maxima are observed, as would be expected due to the stabilisation of the filled metal d-orbitals by the reduction in the σ-donor strength of the protonated triazole ligand. In addition, on protonation of both **1** and **2** the emission lifetime decreases to the sub-nanosecond timescale. This decrease (in

Table 2 Spectroscopic and redox data for complexes described in text

	Abs. λ max/ nm ($\varepsilon/10^{-3}$ M^{-1} cm^{-1})	Em. λ max 298 K/nm	[b]Lifetime at 298 K/ns	[c]Ru^{II}/Ru^{III} oxid. (ligand)/V	Ligand based red./V
[a]$[Ru(bipy)_3]^{2+}$	452	608	1000	1.26	−1.33, −1.55, −1.8
1 $[Ru(bipy)_2(\mathbf{L1})]^{+}$	485 (10.7) 290 (80.7)	685	110	0.80 (1.20, 1.40)	−1.48, −1.76
$[Ru(bipy)_2(\mathbf{HL1})]^{2+}$	441 (15.3) 286 (86.8)	612	—	1.2 (1.45)	*Not measured*
2 $[(Ru(bipy)_2)_2(\mathbf{L2})]^{2+}$	481 (18.9) 290 (148)	683	105	0.82 (1.26, 1.45)	−1.48, −1.73
$[(Ru(bipy)_2)_2\mathbf{HL2}]^{4+}$	412 (28.3) 285 (153)	612	—	1.25 (1.5)	−1.49, −1.73
3 $[Ru(bipy)_2(pytr)]^{+}$	465 (11.0)	650	145	0.83	−1.47, −1.72, −2.25
$[Ru(bipy)_2(pytr)]^{2+}$	437 (12.9)	620	—	1.14	−1.49, −1.73, −2.25
[d]**4** $[(Ru(bipy)_2)_2(bpt)]^{3+}$	453 (22.6)	648	100	1.04, 1.34	−1.40, −1.62, −1.67

[a] From1. [b] Lifetimes measured in deaerated acetonitrile at 298 K (lifetimes for protonated species are sub-nanosecond and were not measured). [c] All redox potentials are *vs.* SCE in 0.1 M TEAP–acetonitrile, 100 mV s^{-1} scan rate. [d] Value obtained from ref. 19.

contravention of the energy gap law[22]) is a result of the reduction in the ^{3}MLCT − ^{3}MC gap, which facilitates fast thermally activated radiationless deactivation of the emissive ^{3}MLCT excited state *via* population of the ^{3}MC state.[21] The acid–base properties of **1** and **2** (pK_a = 4.0 and 4.1, respectively) have been determined using absorption spectroscopy by titration both in Britton–Robinson buffer and in acetonitrile and are similar to those reported previously for **3** (pK_a = 4.07).[21] In the case of complex **2**, a two-step protonation process is possible however only a single protonation step is observed in aqueous media in the range of pH 1.5 to 10 (Fig. 5). Titration in acetonitrile

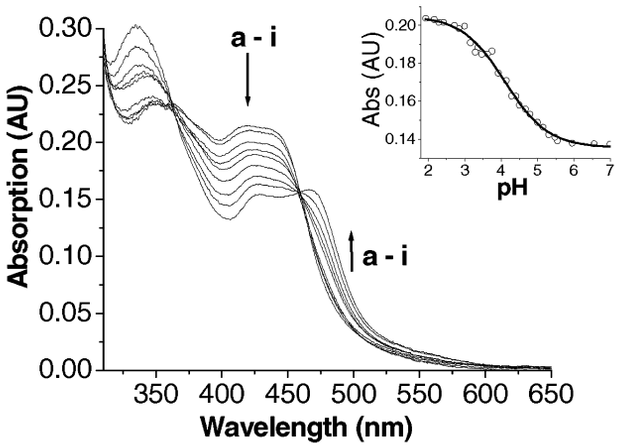

Fig. 5 Titration of **2** in Britton–Robinson buffer pH (a) 1.84; (b) 2.50; (c) 2.84; (d) 3.16; (e) 3.62; (f) 3.92; (g) 4.29; (h) 4.79; (i) 10.06 (inset; pH titration plot monitored at 415 nm).

shows complete protonation with two equivalents of trifluoroacetic acid, indicating that in aqueous media both protonation steps occur at essentially the same pH.

Electrochemical and spectroelectrochemical properties

Redox properties of **1** and **2** are presented in Table 2. $E_{1/2}$ values were determined by cyclic voltammetry (CV). For each of the deprotonated complexes a single reversible redox wave was observed at low oxidation potentials followed by two quasi-reversible oxidation waves at higher potentials. The reversible peaks at 0.8 (**1**) and 0.82 V (**2**) (*vs.* SCE) are attributed to oxidation of the metal centre (*vide infra*), while the quasi-reversible peaks at 1.2 (**1**) and 1.26 V (**2**) are assigned to the first oxidation of the dimethoxyphenyl grouping (Fig. 6). No clear electrochemistry was obtained for the free dimethoxy ligand, most likely because of adsorption on the electrode surface. The metal oxidation potentials are considerably lower (~300 mV) than for $[Ru(bipy)_3]^{2+}$, as is expected for the stronger σ-donating 1,2,4-triazoles. The larger peak-to-peak separation (E_p) in the first oxidation wave of **2** compared with **1** reflects the bi-electronic process involved in the metal oxidation ($Ru^{II}Ru^{II}$ to $Ru^{III}Ru^{III}$). For the protonated complexes all redox waves are observed at a

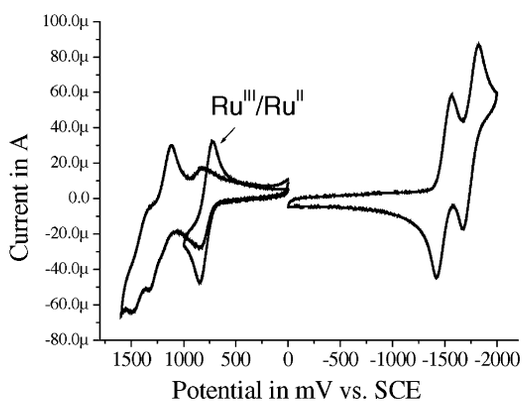

Fig. 6 Cyclic voltammogram of **1** showing reversibility of Ru^{II}/Ru^{III} redox couple and subsequent irreversible ligand oxidation couples (in 0.1 M TEAP–acetonitrile, 100 mV s^{-1} scan rate, ref. SCE).

higher oxidation potential for both **1** and **2**, which arises from the reduced σ-donor capacity of the protonated triazole moieties. Comparison of the first oxidation potential of **2** with those of **1**, **3** and **4**, indicates that $Ru(bipy)_2$(1,2,4-triazole)-units of the dimer behave independently and have properties similar to monomeric species and are quite different from those observed for the dinuclear complex **4**.

The extent of interaction between metal centres in polynuclear complexes has been classified by Robin and Day as Type I, II or III.[23] In dinuclear metal complexes, the metal redox properties are useful in investigating electronic interaction between metal subunits. In principle, because two redox-active sites are present (the two metal centres), two metal-centred oxidation processes are possible, and their separation (ΔE) is related to the stability of the mixed-valence species by the comproportionation constant, K_c, as defined in eqn. 1. The

$$K_c = \exp(\Delta E/25.69) \quad (1)$$

absence of a measurable difference (ΔE < 40 mV) in the two metal-based oxidations of **2** indicates that little or no communication between the metal centres exists, and the value of K_c for **2** is therefore reported to be less than 5.[24]

However, since fast electron transfer between metal centres can occur with an electronic coupling as low as tens of wavenumbers,[10] the absence of two resolvable redox waves does not automatically indicate that the coupling between the metal centres is absent. The most direct measure of the metal–metal electronic coupling in a mixed valence system, $Ru^{II}Ru^{III}$, can be obtained from intervalence transitions (IT).[25,26] For this reason the spectroelectrochemical investigations have been carried out. The electronic properties of partially and completely oxidised complexes, **1** and **2**, together with data from model systems are presented in Table 3.

Applying a potential of 0.8 V (*vs.* pseudo Ag/AgCl reference electrode) to a basic acetonitrile solution of **1** results in

Table 3 Absorption bands observed for complexes **1**, **2** and **4** in Ru^{II}, $Ru^{II}Ru^{III}$ (mixed valence) and Ru^{III} oxidation states

Complex	Ru^{II} MLCT bands/nm (cm^{-1})	$Ru^{II}Ru^{III}$ IT bands/nm (cm^{-1})	Ru^{III} LMCT bands/nm (cm^{-1})
[a]$[Ru(bipy)_3]^{2+}$	452 (22075)	—	675 (14810)
1 $[Ru(bipy)_2(\mathbf{L1})]^{+}$	485 (20620)	—	1075 (9300)
$[Ru(bipy)_2(\mathbf{HL1})]^{2+}$	440 (22725)	—	825 (12120)
2$[(Ru(bipy)_2)_2(\mathbf{L2})]^{2+}$	482 (20745)	1540 (6470)	1220 (8220)
$[(Ru(bipy)_2)_2(\mathbf{H_2L2})]^{2+}$	412 (24270)	—	840 (11930)
4 $[(Ru(bipy)_2)_2(bpt)]^{3+}$	453 (22075)	1800 (5556)	753 (13280)

[a] Value obtained from ref. 27

depletion in the MLCT band at 485 nm, coupled with the formation of a new band at 1075 nm. This band is comparable to the ligand to metal charge transfer bands (LMCT) observed for other $[Ru(LL)_3]^{3+}$ complexes (where LL = substituted-2,2-bipyridine).[27] Upon increasing the oxidation potential to 1.3 V, the depletion of the MLCT band continues, while the band at 1075 nm also decreases in intensity. The depletion of the MLCT bands at 485 nm and the appearance of the LMCT band at 0.8 V is consistent with the oxidation of the metal centre. Further increase of the oxidation potential to 1.3 V is irreversible and results in decomposition of the complex in agreement with data obtained from cyclic voltammetry (*vide supra*). The reversibility of the initial oxidation process has been confirmed by reformation of the initial spectrum upon bulk electrolysis at 0.3 V, subsequent to electrolysis at 0.8 V.

For **2** the situation is similar except that for this compound an additional broad feature at 1545 nm is formed at 0.75 V prior to formation of the expected LMCT absorption band at 1216 nm (Fig. 7). Further oxidation at higher potentials results

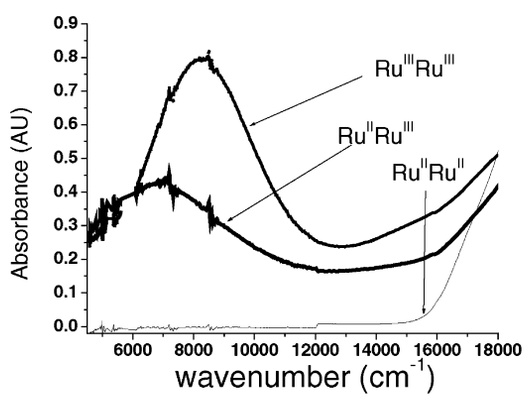

Fig. 7 Near-IR absorption spectra of the fully reduced ($Ru^{II}Ru^{II}$) mixed valence ($Ru^{II}Ru^{III}$) (electrolysis at 0.75 V *vs.* pseudo Ag/AgCl) and full oxidised ($Ru^{III}Ru^{III}$) (electrolysis at 0.85 V *vs.* pseudo Ag/AgCl) complex **2**.

in depletion of all spectroscopic bands as was observed for **1**. The band initially formed at 1545 nm is assigned as an IT band on the basis of its absence in the spectra of **1** and its energy and bandwidth which are comparable to those observed for $[(Ru(bipy)_2)_2bpt]^{4+}$.[19] The depletion of the 1545 nm band and the formation of the LMCT band at higher energy occur with the presence of a sharp isosbestic point at 1490 nm. The situation is similar to that of Bonvoisin *et al.*[28] for the formation of an IT band of an organic aromatic polyamine system, which exhibited a single reversible three electron oxidation wave. Emission-spectroelectrochemistry has also been used to investigate the species, which are present during formation of both IT and LMCT bands of the partially and fully oxidised species, respectively. Oxidation of **2** up to 0.85 V (*vs.* pseudo Ag/AgCl) results in depletion of the emission at 683 nm. The initial emission spectrum completely recovered upon returning the potential to 0.3 V. In contrast when **2** is oxidised at 1.3 V and the potential returned to 0.3 V the original emission spectrum is not reformed rather a new emission is observed at higher energy, indicating irreversible ligand oxidation of **2**. The nature of the product formed was not further investigated.

Under acidic conditions, at which the triazole ring is protonated, no IT band is observed for **2**. The LMCT bands observed are shifted to higher energy compared with the LMCT bands observed for the deprotonated complexes, from 1075 nm to 825 nm for **1** and from 1220 nm to 840 nm for **2**. The intensities of these bands relative to the LMCT bands of the deprotonated complexes is also much reduced. These observations are not unexpected and can be rationalised in terms of the relative energies of the donor (ligand based) and acceptor (metal based) orbitals. The effect of protonation and the subsequent decrease in the σ-donor properties of the bridging ligand is to increase the energy of both the donor and acceptor orbitals leading to the observed shift in the LMCT transition. In addition upon protonation there is a noticeable decrease in the intensity of the LMCT band, which reflects the decreased electron density of the triazole ligands. These results are consistent with the findings of Nazeeruddin *et al.*,[27] who have found that the intensity of the LMCT transition increases with increasing electron-donating capacity of the donor ligand.

Estimation of electronic coupling (H_{ab})

Hush theory may be applied to multinuclear systems exhibiting IT bands in their mixed valence states[25] to quantify the level of interaction between the metal centres of the dinuclear complex. A measure of the interaction between the two metal centres in the mixed valence state can be obtained *via* the determination of the resonance exchange integral H_{ab}, as shown in eqn. 2.[26]

$$H_{ab} = [\alpha^2 \cdot E_{op}{}^2]^{1/2} \quad (2)$$

where α^2 is a measure of the extent of electron delocalisation and can be obtained from the intervalence band using eqn. 3;

$$\alpha^2 = \frac{(4.2 \times 10^{-4}) \cdot \varepsilon_{max} \cdot \Delta\nu_{1/2}}{d^2 \cdot E_{op}} \quad (3)$$

where ε_{max} is the extinction coefficient of the IT band (M^{-1} cm^{-1}), $\Delta\nu_{1/2}$ is the peak width at half maximum, d is the estimated internuclear distance in Å, E_{op} is the maximum of the IT band expressed in cm^{-1}.

As noted above, the absence of two resolvable metal oxidation waves in the CV of **2** indicates that any interaction if present is weak. As a result, it is also expected that K_c will be very small and hence at equilibrium only a small proportion of the total concentration of **2** in solution comprises of the mixed valence species. Since the concentration of the $Ru^{II}Ru^{III}$ species is difficult to accurately calculate, the evaluation of ε_{max} (and thence α^2) can only be approximate. Based on the crystal structure of **1**, the internuclear distance of **2** can be estimated as 12 Å. E_{op} is taken directly from the spectra of the mixed valence species (6470 cm^{-1}) and $\Delta\nu_{1/2}$ is taken as double the width at half maximum of the high energy side of the IT band (5100 cm^{-1}). Assuming a maximum extinction coefficient of 2400 M^{-1} cm^{-1} (that of the IT band of **4**) the upper limit of the

interaction parameter α^2 for the system is found to be 0.0055 cm^{-1} (H_{ab} = 480 cm^{-1}), compared with 0.016 for **4** (H_{ab} = 700 cm^{-1}). This confirms that although an interaction is present it is at most very weak and hence the system is best described as type II. For the protonated complex the absence of an IT band and the single bielectronic redox wave confirms it to be type I *i.e.* no interaction.

Concluding remarks

Complexes **1** and **2** are synthetic intermediates in the preparation of hydroquinone and quinone containing complexes. The present study forms therefore a basis for the investigation of quinone complexes, which will be reported in a later publication. X-Ray and molecular structures of **HL1** and **H_2L2** and of **1** facilitate detailed studies of these and similar compounds with respect to the distance dependence of electron and energy transfer processes in the quinone/hydroquinone target compounds. The electrochemical, acid–base, spectroscopic and photophysical results reported in this study for **1** and **2**, indicate that for the dinuclear species the individual metal centres behave independently and in an almost identical fashion to the mononuclear complex **1**. Importantly they show only a single two electron metal-based oxidation. This indicates that the interaction between the two metal centres is weak. In the deprotonated complex **2** the presence of an intervalence band in the spectroelectrochemical data confirm the presence of a weak interaction. The results obtained show that the electronic interaction (H_{ab}) in **2** is considerable less than observed in **4**. This is not unexpected on the basis of the increased distance (d) between the metal centres and the presence of the 'phenyl spacer', which has been found in previous studies to provide poor electronic communication.[19] This study allows for more successful prediction of the supramolecular aspects of analogous systems containing hydroquinone and quinone moieties where direct electrochemical and spectroelectrochemical investigations are not possible due to the presence of ligand based oxidations at potentials lower than that of the metal centres.[12] The present study is aimed at providing a base for the comparison of the electrochemical and photophysical properties of such compounds and assesses the potential of the hydroquinone/quinone redox couple to act as an electrochemical switch.

Acknowledgements

The authors thank Enterprise Ireland and the EU TMR Grant no. CT96076 for financial assistance.

References

1 A. Juris, V. Balzani, F. Barigelletti, S. Campagna, P. Belser and A. von Zelewsky, *Coord. Chem. Rev.*, 1988, **84**, 85.
2 K. Kalyanasundaram, *Coord. Chem. Rev.*, 1982, **46**, 159.
3 E. A. Seddon and K. R. Seddon, *The Chemistry of Ruthenium*, Elsevier, Amsterdam, 1984, ch. 15.
4 V. Balzani, F. Scandola, *Supramolecular Photochemistry*, Ellis Horwood, Chichester, UK, 1991.
5 *Supramolecular Photochemistry*, ed. V. Balzani, Reidel, Dordrecht, 1997.
6 P. R. Rich, *Faraday Discuss. Chem. Soc.*, 1982, **75**, 349.
7 K. S. Schanze and K. Sauer, *J. Am. Chem. Soc.*, 1998, **110**, 1180.
8 V. Goulle, A. Harriman and J.-M. Lehn, *J. Chem. Soc., Chem. Commun.*, 1993, 1034.
9 K. A. Opperman, S. L. Mecklenburg and T. J. Meyer, *Inorg. Chem.*, 1994, **33**, 5295.
10 V. Balzani, S. Campagna, G. Denti, A. Juris and M. Venturi, *Coord. Chem. Rev.*, 1994, **132**, 1.
11 S. Fanni, T. E. Keyes, S. Campagna and J. G. Vos, *Inorg. Chem.*, 1998, **37**, 5933.
12 T. E. Keyes, P. M. Jayaweera, J. J. McGarvey and J. G. Vos, *J. Chem. Soc., Dalton Trans.*, 1997, 1627.
13 R. Wang, T. E. Keyes, R. Hage, R. H. Schmehl and J. G. Vos, *J. Chem. Soc., Chem. Commun.*, 1993, 1652.
14 B. P. Sullivan, D. J. Salmon and T. J. Meyer, *Inorg. Chem.*, 1978, **17**, 3334.
15 R. Wang, J. G. Vos, R. H. Schmehl and R. Hage, *J. Am. Chem. Soc.*, 1992, **114**, 1964.
16 J. Fait, XSCANS, Program for Data Collection and Processing, 1993, Bruker, Madison, WI.
17 G. M. Sheldrick, SHELXTL version 5.10, University of Gottingen, Germany, 1997.
18 F. Barigelletti, L. De Cola, V. Balzani, R. Hage, J. G. Haasnoot, J. Reedijk and J. G. Vos, *Inorg. Chem.*, 1989, **28**, 4344.
19 R. Hage, J. G. Haasnoot, J. Reedijk, R. Wang, E. M. Ryan, J. G. Vos, A. L. Spek and A. J. M. Duisenberg, *Inorg. Chim. Acta*, 1990, **174**, 77.
20 D. P. Rillema, D. S. Jones, C. Woods and H. A. Levy, *Inorg. Chem.*, 1992, **31**, 2935.
21 R. Hage, A. H. J. Dijkhuis, J. G. Haasnoot, R. Prins, J. Reedijk, B. E. Buchanan and J. G. Vos, *Inorg. Chem.*, 1988, **27**, 2185.
22 T. J. Meyer, *Pure Appl. Chem.*, 1984, 630.
23 M. P. Robin and P. Day, *Adv. Inorg. Chem. Radiochem.*, 1967, **10**, 247.
24 D. E. Richardson and H. Taube, *Inorg. Chem.*, 1981, **20**, 1278.
25 (*a*) N. S. Hush, *Prog. Inorg. Chem.*, 1967, **8**, 391; (*b*) N. S. Hush, *Electrochim. Acta*, 1968, **13**, 1005.
26 C. Creutz, O. N. Marshall and N. Sutin, *J. Photochem. Photobiol., A: Chem.*, 1994, **82**, 47.
27 M. K. Nazeeruddin, S. M. Zakeeruddin and K. Kalyanasundaram, *J. Phys. Chem.*, 1993, **97**, 9607.
28 J. Bonvision, J.-P Launay, M Van der Auweraer and F. C. De Schryver, *J. Phys. Chem.*, 1994, **98**, 5052.